

Article

3D Printing of Hybrid Cements Based on High Contents of Powders from Concrete, Ceramic and Brick Waste Chemically Activated with Sodium Sulphate (Na_2SO_4)

Rafael Robayo-Salazar , Fabio Martínez , Armando Vargas and Ruby Mejía de Gutiérrez * 

Composite Materials Group (GMC-CENM), Universidad del Valle, Cali 760033, Colombia; rafael.robayo@correounivalle.edu.co (R.R.-S.); fabio.martinez@correounivalle.edu.co (F.M.); vargas.armando@correounivalle.edu.co (A.V.)

* Correspondence: ruby.mejia@correounivalle.edu.co

Abstract: This article evaluates the synthesis, characterization and 3D printing of hybrid cements based on high (70%) contents of powders from concrete waste (CoW), ceramic waste (CeW) and red clay brick waste (RCBW) from construction and demolition waste. For the synthesis of the hybrid cements, 30% (by weight) of ordinary Portland cement (OPC) was added. Sodium sulphate (Na_2SO_4) (4%) was used as a chemical activator. The effect of the liquid/solid ratio on the properties in the fresh state of the mixes was studied by means of minislump, flowability index, and buildability tests. The compressive strength was evaluated at 3, 7, 28 and 90 days of curing at room temperature ($\approx 25^\circ\text{C}$), obtaining strengths of up to 30.7 MPa (CoW), 37.0 MPa (CeW) and 33.2 MPa (RCBW) with an L/S ratio of 0.30. The results obtained allowed selecting the CoW 0.30, CeW 0.33 and RCBW 0.38 mixes as optimal for carrying out 3D printing tests on a laboratory scale, successfully printing elements with good print quality, adequate buildability, and compressive strength (CoW 0.30 = 18.2 MPa, CeW 0.33 = 27.7 MPa and RCBW 0.38 = 21.7 MPa) higher than the structural limit (≥ 17.5 MPa) established for concrete by Colombian Regulations for Earthquake Resistant Construction (NSR-10).

Keywords: additive manufacturing; 3D printing; construction and demolition waste; sodium sulphate; alkali-activated materials; geopolymers



Citation: Robayo-Salazar, R.; Martínez, F.; Vargas, A.; Mejía de Gutiérrez, R. 3D Printing of Hybrid Cements Based on High Contents of Powders from Concrete, Ceramic and Brick Waste Chemically Activated with Sodium Sulphate (Na_2SO_4). *Sustainability* **2023**, *15*, 9900. <https://doi.org/10.3390/su15139900>

Academic Editor: José Ignacio Alvarez

Received: 1 June 2023

Revised: 16 June 2023

Accepted: 20 June 2023

Published: 21 June 2023



Copyright: © 2023 by the authors. Licensee MDPI, Basel, Switzerland. This article is an open access article distributed under the terms and conditions of the Creative Commons Attribution (CC BY) license (<https://creativecommons.org/licenses/by/4.0/>).

1. Introduction

The worldwide 3D printing construction market was valued at USD 11 million in 2021 and expected to grow to USD 48 million in 2030, according to Grand View Research [1]. In fact, the implementation of additive manufacturing technology in the construction sector has brought into play a new market and given rise to multiple advantages for this industry compared to conventional construction methods. Among such advantages are a higher construction speed [2], reduced labour costs [3], greater energy efficiency [4], lower consumption of materials [5], decreased waste generation and the possibility of producing elements with complex geometries almost impossible to obtain using conventional methods [6]. As highlighted in [7], factors necessary to position 3D printing as a sustainable construction method include using non-conventional cementitious materials [8], including alkali-activated cements, geopolymers and hybrid cements [9–14].

Synthesis of these non-conventional cementitious materials is based on chemical activation of a material rich in aluminosilicates (precursor) through the use of alkaline activators (hydroxide type (ROH , $\text{R}(\text{OH})_2$), weak acid salts (R_2CO_3), strong acid salts (Na_2SO_4 , $\text{CaSO}_4 \cdot 2\text{H}_2\text{O}$), and siliceous salts $\text{R}_2\text{O}(\text{n})\text{SiO}_2$, where R is an alkaline ion of the Na, K or Li type [15]. This process gives rise to materials with physical, mechanical and durable properties similar or even superior to traditional cementitious materials such as ordinary Portland cement (OPC) [16]. Another advantage of these types of non-

conventional cementitious material is their potential to reduce the carbon footprint, making it possible to call them environmentally friendly cements [17,18].

In particular, hybrid cements are able to use a small amount ($\leq 30\%$) of OPC that promotes a gain of strength at room temperature ($\approx 25\text{ }^\circ\text{C}$) and that can be chemically activated with smaller amounts (2–6% by weight) of Na_2SO_4 (sodium sulphate) [19]. Na_2SO_4 has a lower economic and energy cost than traditional alkaline activators (NaOH (sodium hydroxide) and Na_2SiO_3 (waterglass)) [20]. The chemical activation mechanism of these hybrid cements ($\text{OPC} \leq 30\%$) via incorporation of Na_2SO_4 has been described by other authors [21]. The role of the SO_4^{2-} ion in these non-conventional binders consists of (1) accelerating the hydration process of the alite (C_3S) phase present in the clinker; (2) the formation of ettringite from the reaction with the celite phase (C_3A); and (3) the formation of NaOH as a by-product of the reaction between Na_2SO_4 and Portlandite ($\text{Ca}(\text{OH})_2$) generated during the hydration of calcium silicates (C_3S (alite) and C_2S (belite)) present in the clinker. An additional hypothesis derived from these reactions is that the $\text{Ca}(\text{OH})_2$ and NaOH formed can alkaline-activate the reactive phase of the precursor (aluminosilicate) and form (N,C)-A-S-H type hybrid gels [21].

Precursors that can be used for the synthesis of alkali-activated materials include a wide range of pozzolanic additions (Supplementary Cementitious Materials (SCM)) of natural or artificial origin, and industrial by-products with high aluminosilicate contents, including natural pozzolans, fly ash, steel slag and thermally activated clays (metakaolin), among others. Construction and demolition waste (CDW) is made up mostly of concrete waste (CoW), ceramic waste (CeW) and red clay brick waste (RCBW). All of these are aluminosilicate in nature, so they feature a certain degree of reactivity to equally be used as precursors. In this regard, in previous studies [22,23], it was shown that the fine fractions (powders) of CDW can be used through chemical activation processes in the synthesis of alkali-activated materials, geopolymers and/or hybrid cements.

According to Raza et al. [11], the use of alkali-activated materials in 3D printing was introduced in 2016 by Xia and Sanjayan [14], and from that moment this research topic quickly became an innovative trend for research groups around the world. The application of CDW-based alkali-activated materials however in the field of 3D printing has hardly been explored at all. As highlighted in [7], regardless of its nature, the cementitious material suitable for 3D printing must have an adequate extrusion capacity (mouldable and extrudable material), be fluid, be buildable, with an adequate setting time (open time), have dimensional stability (low shrinkage), and achieve a certain level of mechanical strength to be used in structural applications. In this context, Şahin et al. [24] studied the rheological properties for 3D printing of geopolymers based on hollow brick (HB), red clay brick (RCB), roof tile (RT) and glass (G), activated with combinations of sodium hydroxide (NaOH), calcium hydroxide ($\text{Ca}(\text{OH})_2$) and sodium silicate (Na_2SiO_3). The mix activated with 6.25 M NaOH and 10% $\text{Ca}(\text{OH})_2$ exhibited the best rheological and mechanical properties and was selected for laboratory-scale 3D printing tests. Based on that study [24] and using the same geopolymeric cement, Ilcan et al. [25] demonstrated the possibility of incorporating a fine aggregate of recycled concrete (aggregate-to-binder ratio of 0.38) in the production of low and high viscosity mortars, successfully applying the aggregate in 3D printing without affecting the rheological and mechanical properties of the mortar mixes. Demiral et al. [26] subsequently evaluated the effect of anisotropy (dependence on the direction of 3D printing) on compressive strength in three directions (perpendicular, parallel and lateral) and flexural strength in two directions (perpendicular and lateral), in the geopolymeric mortars produced in the abovementioned study [25]. They further evaluated the adhesion between layers through direct and indirect traction tests. The authors conclude that interlayer adhesion influences the anisotropic behaviour of 3D printed elements. They state however that 3D-printed specimens tested in the direction perpendicular to the printing direction showed similar performance to mould-casted specimens, indicating that interlayer adhesion had little influence in the perpendicular loading direction.

Despite the recent advances, the use of low economic, low energy cost alternative activators such as sodium sulphate (Na_2SO_4) in the synthesis of hybrid cements based on high CDW contents and their application in 3D printing has not yet been reported. This article aims to synthesize and characterize hybrid cements based on high contents (70% by weight) of concrete waste (CoW), ceramic waste (CeW), and red clay brick waste (RCBW), derived from the fine fraction (powder) of construction and demolition waste (CDW), and ordinary Portland cement (OPC) (30% by weight). Na_2SO_4 was used for the chemical activation of the hybrid cements. The effect of the liquid/solid (L/S) ratio on the properties of the fresh state (mini slump, flowability index, workability, and open time) and hardened state (compressive strength) of the mixtures was evaluated, and the optimal ranges of these properties were determined for their application in 3D printing. The optimal mixtures were used in laboratory-scale printing tests, demonstrating their potential application in additive manufacturing processes. These are the first reported results of 3D printing for this type of hybrid cement based on CDW powders.

2. Materials and Methods

2.1. Raw Materials

Concrete waste (CoW), ceramic waste (CeW) and red clay brick waste (RCBW) from construction and demolition activities (CDW) were used to produce the mixes. These residues were finely ground using a ball mill. The particle size was estimated by laser granulometry using a Mastersizer-2000 equipment (Malvern Panalytical, Madrid, Spain). For the synthesis of hybrid cements, ordinary Portland cement (OPC) was used. An Ultrapyc 3000 helium pycnometer (Anton Paar, Graz, Austria) was used to determine the density of the raw materials. The chemical composition was determined by X-ray fluorescence (XRF) using a MagiX-Pro PW-2440 spectrometer (Phillips, Eindhoven, The Netherlands). Industrial grade sodium sulphate (Na_2SO_4) was used for chemical activation of hybrid cements produced.

2.2. Production of Mixes and Characterization

A total of 10 mixes (hybrid cements) (Table 1) were designed based on a 70% precursor content (CoW, CeW or RCBW) and the addition of 30% (by weight) of OPC. In order to evaluate the effect of the liquid/solid (L/S) ratio on the fresh and hardened properties of the mixes, this design variable was modified between 0.30–0.38. For the calculation of the L/S ratio, liquids correspond to the mixing water and solids correspond to the sum of the waste and the OPC (precursor). The Na_2SO_4 content was 4% by weight with respect to the precursor (waste + OPC). The determination of this optimal content (4% by weight) of chemical activator (Na_2SO_4) was based on a previous study [19].

Table 1. Design of mixes and proportioning of raw materials.

| Mix | L/S Ratio | Proportion (g) | | | |
|-----------|-----------|----------------|-----|--------------------------|-------|
| | | Waste | OPC | Na_2SO_4 | Water |
| CoW 0.30 | 0.30 | 70 | 30 | 4 | 30 |
| CoW 0.33 | 0.33 | 70 | 30 | 4 | 33 |
| CoW 0.36 | 0.36 | 70 | 30 | 4 | 36 |
| CeW 0.30 | 0.30 | 70 | 30 | 4 | 30 |
| CeW 0.33 | 0.33 | 70 | 30 | 4 | 33 |
| CeW 0.36 | 0.36 | 70 | 30 | 4 | 36 |
| RCBW 0.30 | 0.30 | 70 | 30 | 4 | 30 |
| RCBW 0.33 | 0.33 | 70 | 30 | 4 | 33 |
| RCBW 0.36 | 0.36 | 70 | 30 | 4 | 36 |
| RCBW 0.38 | 0.38 | 70 | 30 | 4 | 38 |

The mixes were produced in a Hobart mixer with a mixing time of 5 min. Initially, the waste (precursor) was dry homogenized with the addition of OPC. Subsequently, the chemical activator, previously dissolved in the mixing water, was added to the mix.

In order to correlate the rheological behaviour of hybrid cements with their 3D printing capacity, the mixes were characterized in the fresh state by adapting minislump, flow rate and buildability tests. The minislump (Figure 1a) was determined as the settlement shown by the mix due to its own weight after removing the conical mold according to ASTM C230 standard [27].

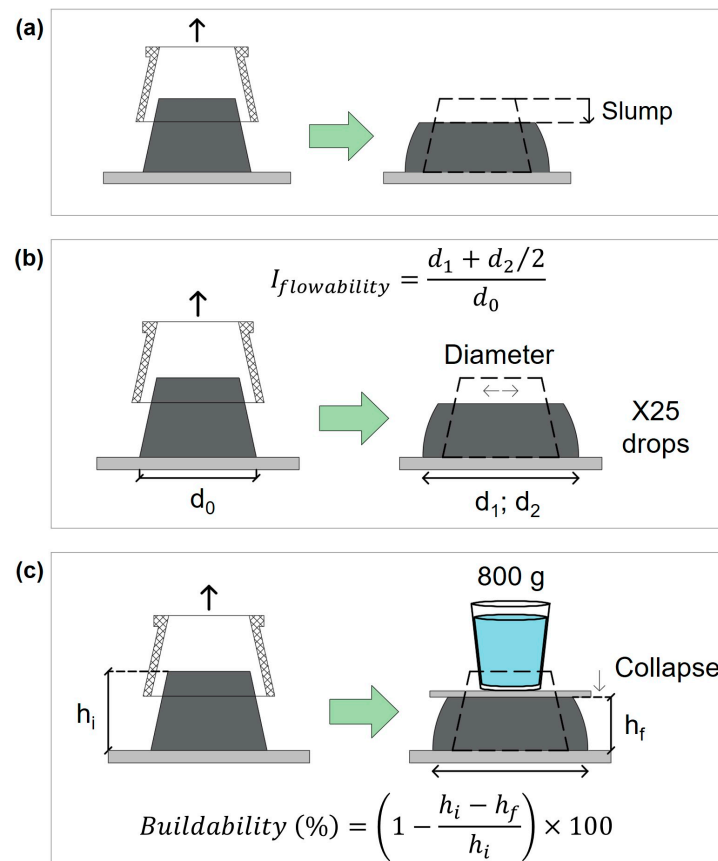


Figure 1. Characterization tests in the fresh state of the mixes: (a) minislump, (b) flowability index and (c) buildability of the mixes.

Flowability index (Figure 1b) was determined according to the procedure established in ASTM C230 [27], taking into account the average diameter reached by the mix after being subjected to 25 drops from the flow table. Buildability (Figure 1c) was determined from the collapse caused by an 800 g weight placed on the mix immediately after carrying out the minislump test. This weight (800 g) is equivalent to the fresh weight of the mix used to fill the conical mould.

The setting time (initial and final) of the mixes was determined according to the procedure described in the ASTM C191 standard (method B) [28] using a Vicat apparatus. Additionally, the effect of setting time on ultrasonic pulse velocity was evaluated using a Pundit PL-200 unit (Proceq, Schwerzenbach, Swiss) with P-type wave transducers of 54 kHz frequency, a pulse voltage of 200 V, and a sensor gain of 500×. For the measurement of ultrasonic pulse velocity in the fresh state, an acrylic cubic mould with a side of 75 mm and a wall thickness of 1.3 mm was used. Additionally, the effect of mixing time on the loss of workability of the mixes was established through the minislump and flowability tests. This evaluation was carried out up to a maximum mixing time of 90 min. Together, these tests allowed us to study the open time of the mixes for 3D printing.

The compressive strength of the hybrid cements was evaluated in an INSTRON 3369 (Instron, Norwood, MA, USA) universal testing machine with a 50 kN capacity, using a testing speed of 1 mm/min. Conventionally moulded 20 mm cubes were tested to calculate the average strength of the mixes at 3, 7, 28 and 90 days of curing at room temperature (25 °C) (relative humidity (RH) \approx 80%). Each value of strength corresponds to the average of three test samples.

2.3. Additive Manufacturing (3D Printing) and Tests

The additive manufacturing process carried out is summarized in Figure 2, starting with the computer-aided design (CAD) of a solid part exported in .STL format, followed by the printing parameterization process through the free software Ultimaker Cura 5.0 and generating a file in .gcode format. Finally, the execution of the printing process was carried out using a Creality Ender-3 printer (Creality, Shenzhen, China), to which a Ceramic 3D Printer Kit (Eazao) was adapted. The optimum printing speed was 7 mm/s. The nozzle used corresponds to a circular geometry of 8 mm in diameter. The parameterization of the 3D printing process included a layer height of 6 mm, with the layer height/width ratio being 0.75 (6 mm/8 mm). This optimum ratio (0.75) was determined following preliminary printing tests.

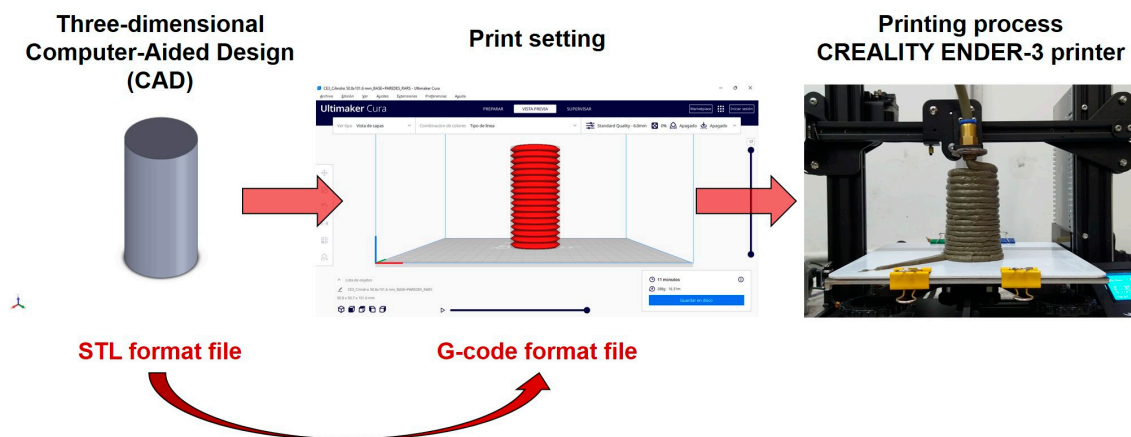


Figure 2. Graphic summary of the methodology followed for the additive manufacturing process (3D printing).

To evaluate the printability of the mixes, hollow (without filling) cylindrical specimens of 50.8 mm in diameter \times 101.6 mm in height (17 layers) were printed (Figure 2). At the end of the printing tests, the actual heights of the 3D specimens were verified with the help of a metric rule to validate their buildability.

Solid beam-type specimens of 45 mm \times 30 mm \times 140 mm (width \times height \times length) were printed to evaluate the mechanical strength (compressive and flexural) of the 3D printed mixes. A total of 3 solid beams were produced for each mix. A concentric filling pattern (from outside to inside) was used, considering 100% filling. The specimens were removed from the impression base (plate) 24 h after their production and were subjected to a curing process in a controlled environment (RH \approx 80% and 25 °C) until the corresponding test age.

The beams were flexural tested (3 points) after 7 days and the compressive strength was determined at 7 and 28 days with the halves of the flexural test beams (Figure 3), according to the procedure described in the UNE-EN 1015 standard [29]. The direction of application of the flexural and compressive loads was perpendicular to the direction of printing (Figure 3). Additionally, the density, absorption and porosity at 28 days were determined according to the ASTM C642 standard [30] from beams of the same type.

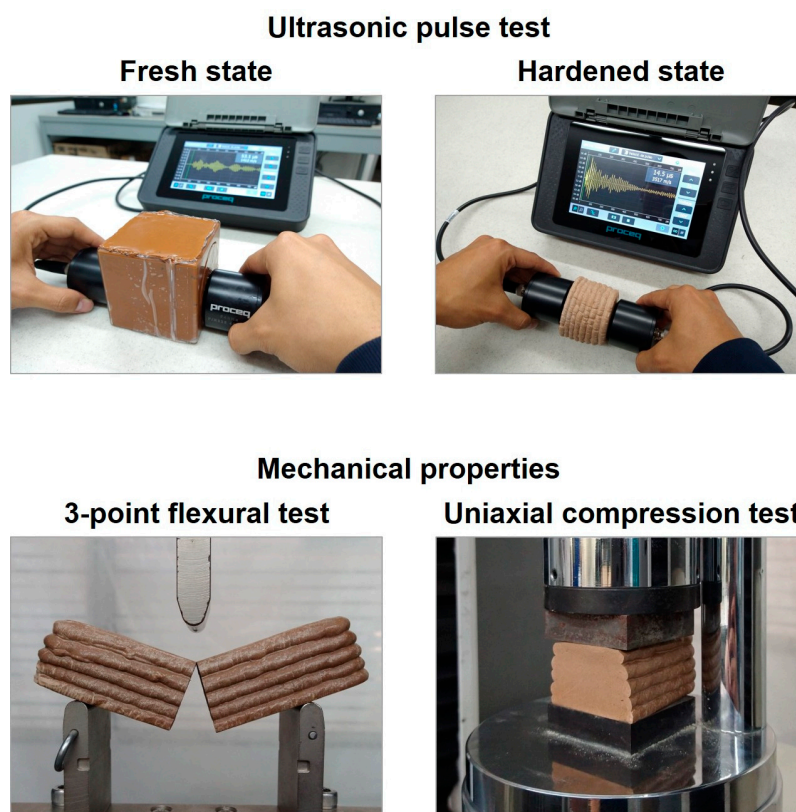


Figure 3. Characterization tests in the hardened state of the mixes: 3D printed specimens.

The ultrasonic pulse velocity was determined at 28 days on solid 3D-printed cylinders 50.8 mm in diameter and 50.8 mm in height according to the procedure established in ASTM C597 [31]. These results were compared with that obtained in specimens made using the conventional casting process (mould-casted). A Pundit 200 instrument was used with P-wave transducers of 54 kHz frequency, a pulse voltage of 100 V and a sensor gain of $1 \times$. Before the measurements, a calibration of the wave transmission time was carried out with the calibration pattern of the equipment. The specimens were tested in a dry condition (ambiently dried). The measurements were made on the lower and upper faces of the specimens (direction perpendicular to the printing direction) (Figure 3). The ultrasonic pulse velocity reported for each mix corresponds to the average of three measurements.

The macroscopic observation of the interface zone between layers was carried out through the inspection of a cross section of the 3D printing specimens in a stereomicroscope. The microstructural analysis was performed on this same area by means of scanning electron microscopy (SEM), using a JEOL JSM-6490LV microscope (Jeol, Tokio, Japan) with an accelerating voltage of 20 kV. An Oxford Instruments Link-Isis X-ray spectrometer was coupled to the microscope (EDS).

3. Results and Discussion

3.1. Materials Characterization

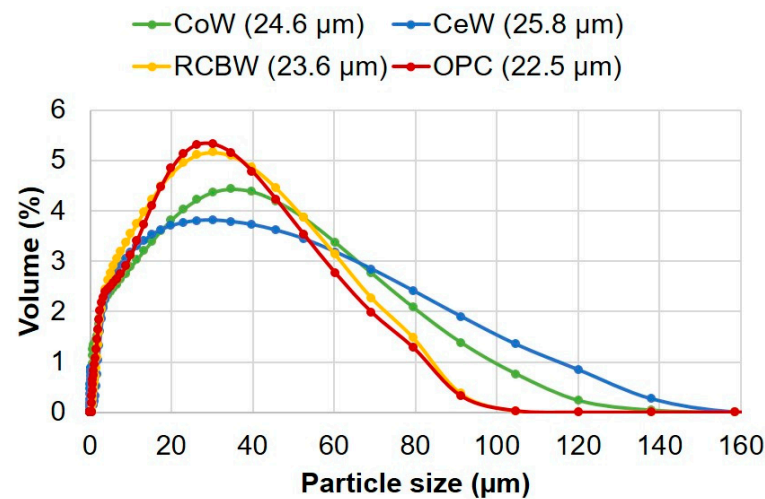
The results of the chemical composition demonstrate the aluminosilicate nature ($\text{SiO}_2 + \text{Al}_2\text{O}_3$) of the CoW, CeW and RCBW, representing 44.4, 75.4 and 77.4% of their total composition, respectively (Table 2).

The densities of the CoW, CeW and RCBW were 2.68, 2.71 and 2.75 g/cm^3 , respectively. The OPC meanwhile reported a density of 3.00 g/cm^3 . The average particle size of the CoW, CeW and RCBW was 24.6, 25.8 and 23.6 μm , respectively (Figure 4). The average particle size of the OPC was 22.5 μm .

Table 2. Chemical composition of raw materials (XRF).

| Material | SiO ₂ | Al ₂ O ₃ | CaO | Fe ₂ O ₃ | MgO | Na ₂ O | K ₂ O | Others | LOI ¹ |
|----------|------------------|--------------------------------|------|--------------------------------|-----|-------------------|------------------|--------|------------------|
| CoW | 36.1 | 8.3 | 28.7 | 6.8 | 1.9 | 0.6 | 0.6 | 1.1 | 15.9 |
| CeW | 59.3 | 16.1 | 9.8 | 5.5 | 0.8 | 0.5 | 1.6 | 2.3 | 4.1 |
| RCBW | 59.0 | 18.4 | 5.4 | 7.8 | 2.4 | 1.1 | 1.5 | 1.5 | 2.9 |
| OPC | 19.4 | 4.1 | 55.7 | 4.7 | 1.7 | 0.3 | 0.3 | 4.6 | 9.2 |

¹ Loss on ignition (LOI)

**Figure 4.** Particle size distribution (laser granulometry) of the materials.

3.2. Fresh Properties

3.2.1. Minislump, Flow Rate and Buildability

The effect of the L/S ratio on the properties in the fresh state of the CoW, CeW and RCBW mixes, included in Table 1, can be seen in Figure 5 (minislump), Figure 6 (flowability index) and Figure 7 (buildability). In general, it is observed that the higher the L/S ratio, the higher the workability (minislump and flowability) of the mixes and as a consequence the lower the buildability, a behaviour that has been reported elsewhere [32]. According to Tay et al. [33], a high water content reduces the internal frictions between the cement particles and resulting in greater flowability. Additionally, it is evident that waste type exerts some control over the rheology of the mixes, suggesting that optimization of each mix design must consider the properties in the fresh state that the type of waste fosters and the effects of these on the 3D printing process. In this regard, the CoW mixes tend to be the most flowability (lowest water demand), followed by the CeW mixes and then the RCBW mixes; the latter demand a higher L/S ratio (0.38) to achieve the level of workability required by the 3D printing process.

In the case of the minislump (Figure 5) and flowability (Figure 6), the CeW 0.30 and RCBW 0.30 and 0.33 mixes have a very dry consistency and fall below the optimal printing region. In relation to the above, the mixes must have an acceptable extrusion capacity, which is affected by a very dry consistency. In contrast, the CoW 0.36 mix had a very fluid consistency that places it above the optimal printing area. Regarding buildability (Figure 7), the very fluid mixes reported a low shape retention capacity (buildability < 80%), which affects the ability to support the weight of the subsequent layers without collapsing and this behaviour is not adequate for the 3D printing process. In contrast, the very dry mixes presented a high buildability (close to 100%), but at the same time a low extrusion capacity (equally unsuitable for 3D printing). In conclusion, it was necessary to find a balance between flowability and buildability in selecting the optimal mixes. Considering this, only the mixes with minislump between 10–20 mm, flowability index between 2.0–2.4 and buildability greater than 80% could be used in the 3D printing process. These correspond

to mixes CoW 0.30; CeW 0.33 and RCBW 0.38. The results of the printing tests of these mixes are included in Section 3.4.1.

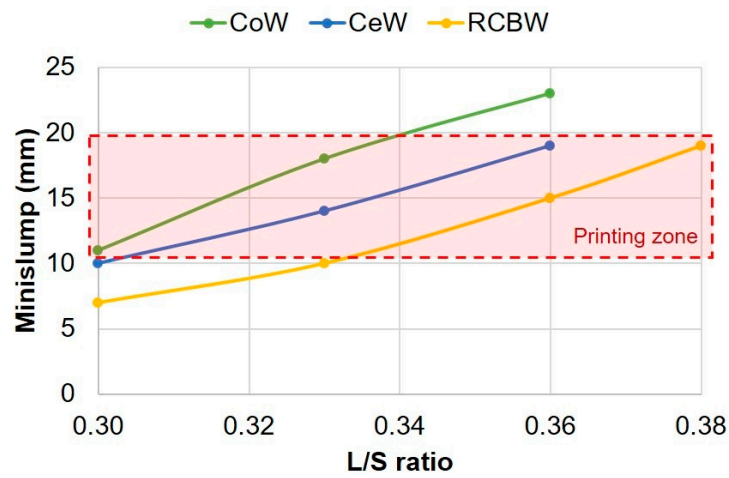


Figure 5. Minislump of the mixes.

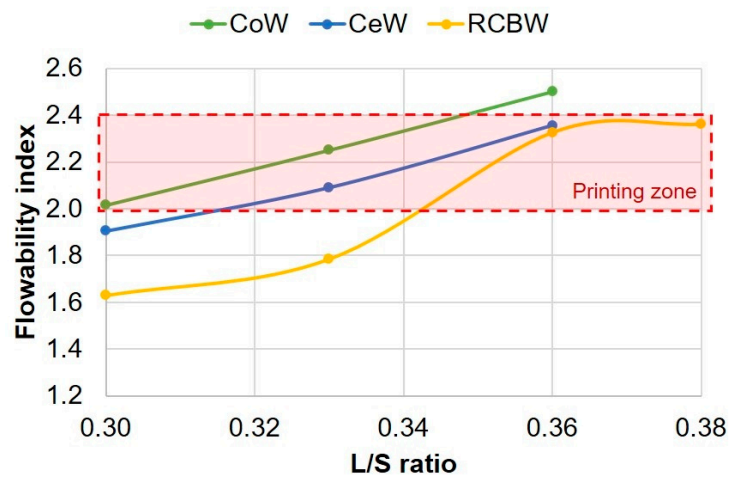


Figure 6. Flowability index of the mixes.

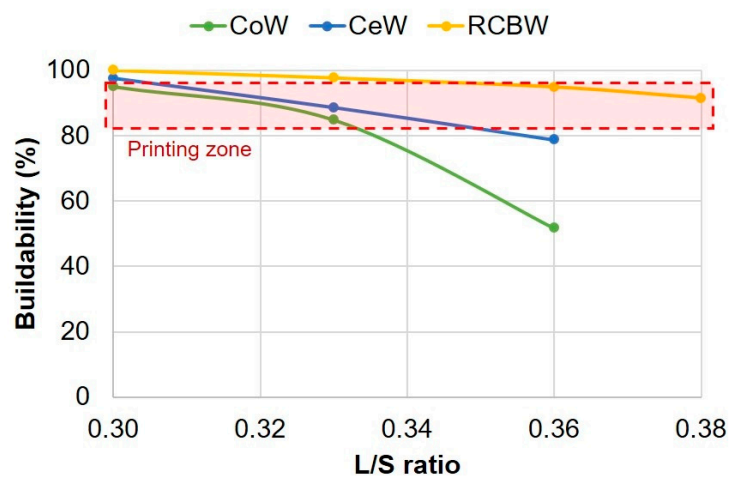


Figure 7. Buildability of the mixes.

3.2.2. Open Time

Open time is defined as the time interval in which the mix is able to be printed before its properties in the fresh state are altered [34]. 3D printing actually requires a sufficient setting time to maintain the consistency of the mix during the extrusion, pumping and deposition process, and thus avoid possible blockages in the pipe and/or nozzle of the printer. However, at the same time a mix with adequate buildability is required; a property that is promoted with short setting times that ensure the necessary strength for the lower layers to support the weight of the upper layers. The open time adjustment must also take into account that a very short setting time could affect adhesion between layers and therefore the mechanical strength of the printed element [2]. Given the above, the effect of L/S ratio on the setting time of the mixes is presented in Figure 8.

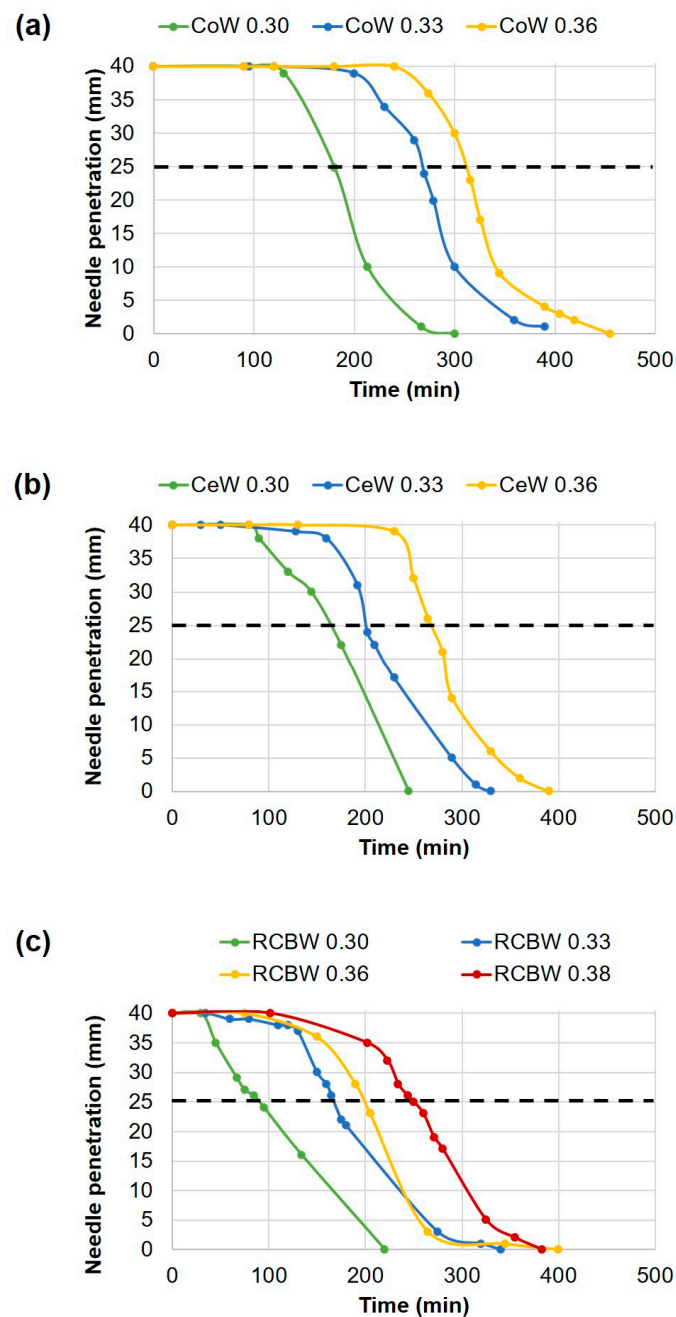


Figure 8. Curves of setting time of the mixes: (a) CoW, (b) CeW and (c) RCBW.

In general, it can be seen that the higher the L/S ratio, the longer the setting time of the mixes. It is also possible to identify that waste type influences initial and final setting times of the mixes. The shortest times are registered for RCBW mixes, followed by CeW mixes and CoW mixes, with the longest times. The RCBW 0.30, 0.33, 0.36 and 0.38 mixes recorded initial setting times of 80, 170, 200 and 250 min, respectively. The CeW 0.30, 0.33 and 0.36 mixes had initial setting times of 160, 200 and 270 min, respectively, while the CoW 0.30, 0.33 and 0.36 mixes reported respective initial setting times of 180, 270 and 310 min.

Ultrasonic pulse velocity monitoring, according to Uppalapati et al. [35], is sensitive to hydrate formation and microstructural changes associated with the setting—hardening—of cementitious materials. Figure 9 relates the ultrasonic pulse velocity of the CoW 0.30, CeW 0.33 and RCBW 0.36 mixes during their setting process. It should be recalled that these mixes were selected as optimal during the evaluation of their properties in the fresh state (Section 3.2.1) and featured initial setting times of 180 min (CoW 0.30), 200 min (CeW 0.33), and 250 min (RCBW 0.38). In Figure 9 a direct correlation is seen between the hardening process of the mixes and the ultrasonic pulse velocity reported, steadily increasing as the mix gradually sets. The ultrasonic pulse velocity for the RCBW 0.38, CeW 0.33 and CoW 0.30 mixes in the initial setting time (needle penetration = 25 mm) were ≈ 1365 , ≈ 1340 and ≈ 1510 m/s, respectively. These values coincide with those reported elsewhere [35] for alkali-activated materials during the initial setting time (1450–1550 m/s). Values above 1650–1750 m/s meanwhile are normally associated with the final setting time of cementitious materials.

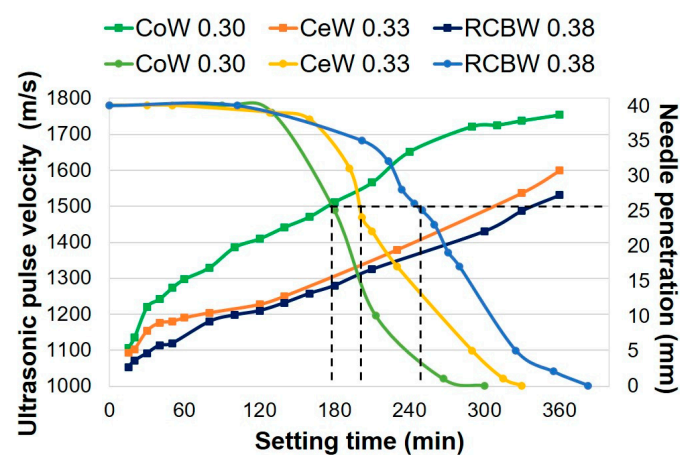


Figure 9. Evolution of ultrasonic pulse velocity as a function of setting time of the CoW 0.30, CeW 0.33 and RCBW 0.38 mixes.

Furthermore, it can be seen in Figure 9 that the ultrasonic pulse velocity curves have the greatest slope (acceleration) during the first minutes (10–40 min). This demonstrates that, before the initial setting, the mixes underwent important changes in their microstructure and properties in the fresh state (flowability), even though with the Vicat needle there were no changes in depth of needle penetration (≈ 40 mm) in that same time interval (10–40 min). This finding allows to conclude that the conventional setting time test (apart from Vicat) is not the most appropriate method to study the open time of mixes for 3D printing and that it is necessary to use other techniques, such as ultrasonic pulse, for more detailed monitoring of reaction kinetics and changes in the fresh state. In this regard, the changes in the velocity of the ultrasonic pulse during the first minutes can be associated with the stages of dissolution (Step I), flocculation (Step II), gelation (Step III) and polycondensation (Step IV) [36]. These stages occur during the hydration process of hybrid cements as consequence of the chemical activation [21].

As mentioned in [7], the open time is usually less than the initial setting time (needle penetration = 25 mm); its experimental evaluation, via tests of loss of flowability as a function of time, is important. Extending the mixing time during 3D printing tests extends

the open time of the mixes, while maintaining the mixes static following the completion of the initial mixing process reduces their useful life. The effect of mixing time (up to 90 min) on the minislump and flowability index of the mixes is thus presented in Figures 10 and 11, respectively.

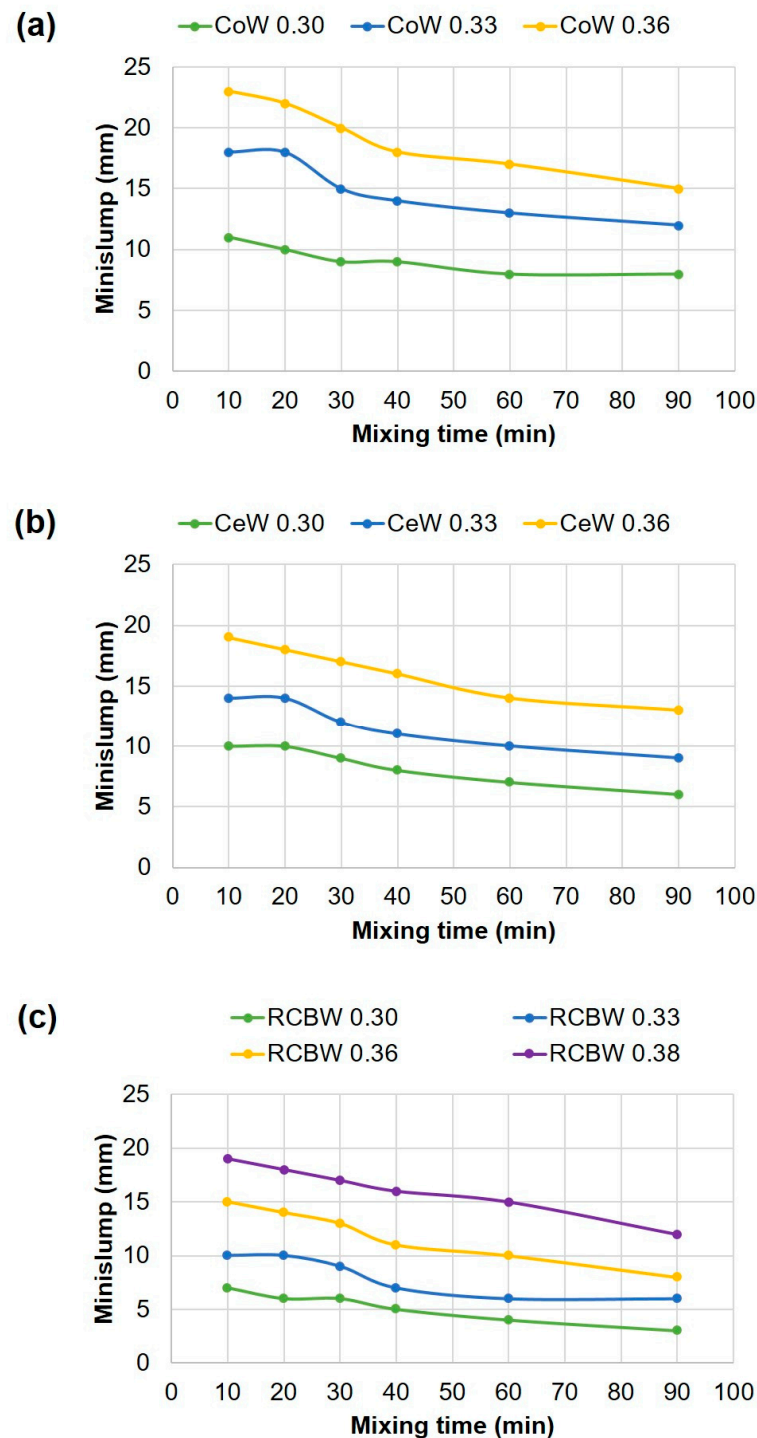


Figure 10. Effect of mixing time on the minislump of the mixes: (a) CoW, (b) CeW and (c) RCBW.

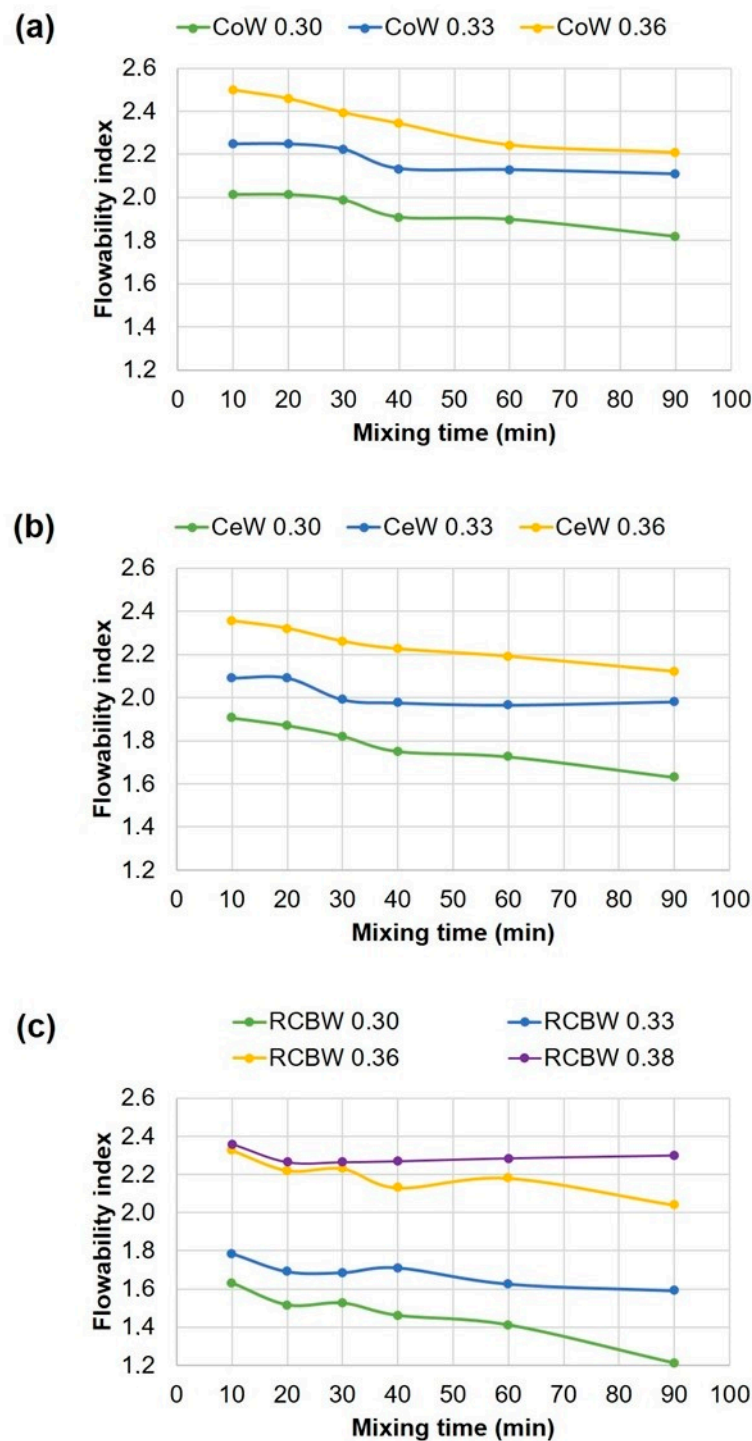


Figure 11. Effect of mixing time on the flowability index of the mixes: (a) CoW, (b) CeW and (c) RCBW.

It was generally observed that after 10–30 min of mixing, the mixes suffered a notable loss of workability (minislump and flowability) and therefore of their 3D printing capacity, results that agree with those reported by Ilcan et al. [25], Zhang et al. [37] and those of commercial products such as Sikacrete-751 3D, Sikacrete-752 3D and Sikacrete-7100 3D [38]. In conclusion, based on the results obtained in this study, it was established that the open times of the CoW 0.30, CeW 0.33 and RCBW 0.38 mixes were 30, 20 and 10 min, respectively.

3.3. Compressive Strength of the Mixes

The evolution of the compressive strength of the CoW, CeW and RCBW mixes is presented in Figure 12. In general, it is observed that the highest mechanical strengths are promoted at lower L/S ratios. Indeed, the maximum compressive strengths (90 days) of the CoW, CeW and RCBW mixes were obtained with an L/S ratio of 0.30 and achieved values of 30.7, 37.0 and 33.2 MPa, respectively.

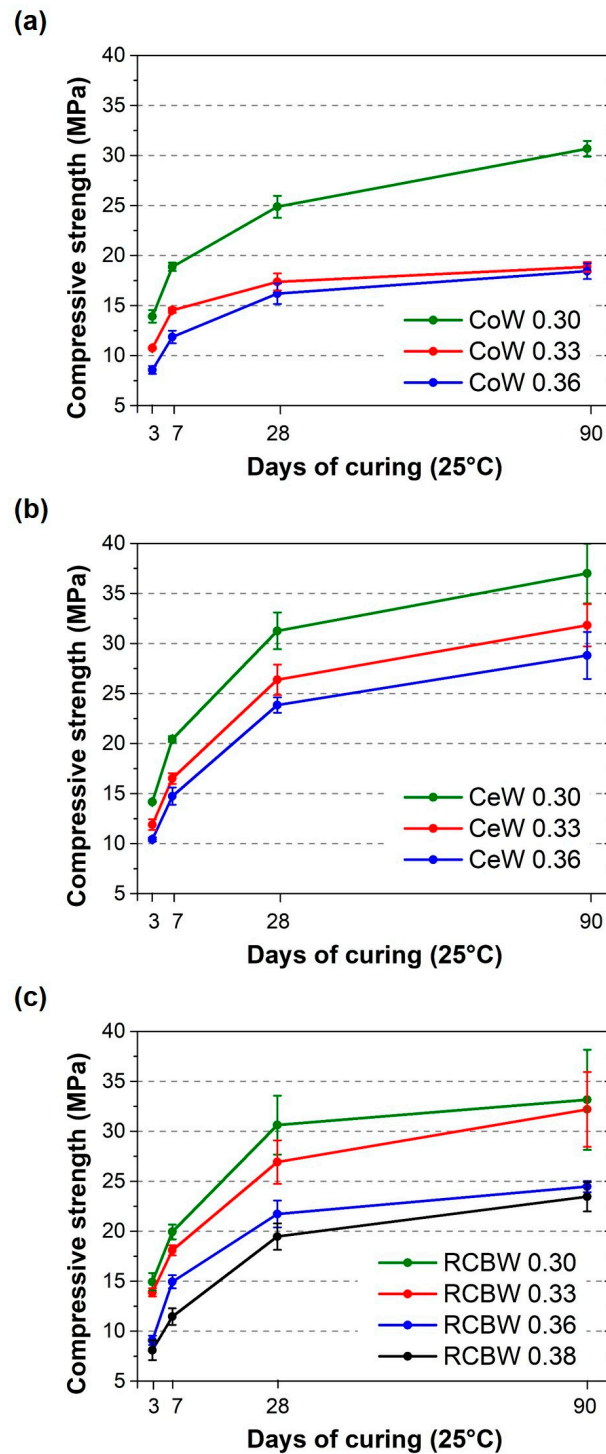


Figure 12. Evolution of the compressive strength of the mixes (3, 7, 28 and 90 days of curing): (a) CoW, (b) CeW and (c) RCBW.

It is evident meanwhile that waste type influences the mechanical performance of the mixes, and this may be related to the degree of chemical reactivity of each material. It should be noted that, in this study, the effect of particle size was controlled and a very similar average size and granulometric distribution was ensured for the three wastes (Figure 4). In this regard, controlling the particle size is considered fundamental for comparative purposes, since this property has a strong influence on the degree of reactivity of the precursor. Clarifying the above, the best mechanical performances for the same L/S ratio were produced by the CeW, followed by the RCBW and lastly the CoW. These mechanical results agree with those reported in other studies [22,23] using residues of the same nature (CDW) and alkaline activation processes.

Regarding the mechanical behaviour of the three mixes previously selected as optimal for the 3D printing process, their compressive strengths were 24.9 MPa (CoW 0.30), 26.4 MPa (CeW 0.33) and 19.5 MPa (RCBW 0.38) at 28 days of curing and 30.7 MPa (CoW 0.30), 31.8 MPa (CeW 0.33) and 23.5 MPa (RCBW 0.38) at 90 days of curing. In the case of the CeW and RCBW mixes, the optimal L/S ratios in the fresh state (0.33 and 0.38) do not coincide with the L/S ratio that promotes the best mechanical performance (0.30). This conflict has been described by other authors [2], recognizing that, in some cases, the need to obtain a fluid mix for 3D printing demands a high mixing water content (high L/S ratio) and this affects the compressive strength of the mixes. This was the case for the RCBW 0.38 mix, which reported the lowest mechanical performance among the mixes optimized for the 3D printing process.

3.4. 3D Printing Tests

3.4.1. Printability and Buildability

In order to validate the application potential of the mixes previously defined as optimal (CoW 0.30; CeW 0.33; RCBW 0.38), the extrusion and 3D printing capacity at laboratory scale was evaluated according to the parameters described in the methodology (Section 2.3). Figure 13 shows the results of this 3D printing test, which correspond to the printing of hollow (without filling) cylinders of 50.8 mm in diameter \times 101.6 mm in height (equivalent to 17 layers of 6 mm thickness). As can be seen, in general, all three mixes were found to have an adequate extrusion and 3D printing capacity, obtaining homogeneous portions and a good surface finish, without the presence of defects, discontinuities (breaks) and/or macro-pores that may compromise the aspect or appearance of the printed element. Some small defects can be seen on the surface of the specimens corresponding to CoW, however these do not compromise the final properties of the element.

Additionally, the buildability of the three mixes was verified by measuring the actual height of the 3D printed cylinders. The results show a high level of buildability (close to 97–99%), in accordance with the characterization in the fresh state previously reported (Figure 7). This result is considered important, since a high degree of fresh deformation (low buildability) can affect the final height of the element compared to the initial model. This difference would lead to an adjustment of the height of the element through the computerized design (CAD) of the part and the parameterization (G-code) necessary to execute the 3D printing process, altering the number of layers.

3.4.2. Physical-Mechanical Behaviour

Table 3 presents the density, absorption and porosity results for the 3D printed specimens corresponding to the CoW 0.30, CeW 0.33 and RCBW 0.38 mixes. As can be seen, the L/S ratio has a significant influence on the physical properties. The higher the L/S ratio, the higher the absorption and the porosity and therefore the lower the density of the 3D specimens obtained. The RCBW 0.38 mix reported the lowest apparent density value (1.92 g/cm³), followed by CeW 0.33 (1.96 g/cm³) and finally CoW 0.30 (1.97 g/cm³) with the highest reported apparent density.



Figure 13. 3D printing and buildability tests of the CoW 0.30, CeW 0.33 and RCBW 0.38 mixes.

Table 3. Density, absorption and porosity of the 3D printed specimens (ASTM C642) [30].

| Mix | Absorption (%) | Bulk Density, Dry (g/cm ³) | Apparent Density (g/cm ³) | Permeable Pore Volume (%) |
|-----------|----------------|--|---------------------------------------|---------------------------|
| CoW 0.30 | 26.9 | 1.55 | 1.97 | 42.4 |
| CeW 0.33 | 28.5 | 1.52 | 1.96 | 43.9 |
| RCBW 0.38 | 32.6 | 1.44 | 1.92 | 47.6 |

Regarding the mechanical characterization of the 3D printed specimens, Table 4 presents the results of flexural (7 days) and compressive strength (7 and 28 days). In this regard, the highest compressive strength was reported by the CeW 0.33 mix, achieving a value of 27.7 MPa at 28 days. The RCBW 0.38 and CoW 0.30 mixes meanwhile attained values of 21.7 MPa and 18.2 MPa at 28 days, respectively. It should be noted that these values are above the structural limit (17.5 MPa) established for concrete mixes according to the Colombian Regulations for Earthquake Resistant Construction (NSR-10).

Table 4. Flexural and compressive strength of the 3D printed specimens.

| Mix | Flexural Strength (MPa) | Compressive Strength (MPa) | |
|-----------|-------------------------|----------------------------|---------|
| | 7 Days | 7 Days | 28 Days |
| CoW 0.30 | 4.9 | 11.5 | 18.2 |
| CeW 0.33 | 4.6 | 12.7 | 27.7 |
| RCBW 0.38 | 4.4 | 10.5 | 21.7 |

Meanwhile, the results of compressive strength of the 3D specimens coincide with the previously reported mechanical performance at the paste level (CeW > RCBW > CoW). It should be noted that, in the present study, the effect of the direction of the test on the compressive strength of the 3D printed specimens was not evaluated. However, some authors [26,39] show that in the direction of test used (perpendicular to the printing direction) the highest strength values are obtained.

Regarding the flexural strength (7 days) of the 3D printed specimens, it is evident that the reported values fluctuated between 4.4 and 4.9 MPa, these values being equivalent to 36.2–42.6% of the reported compressive strength of the 7 days of curing with these same mixes. In conventional concrete, this equivalence (flexural/compressive) is lower and normally ranges between 10–20% of the compressive strength. According to Kaliyavaradhan et al. [34], the perpendicular test direction, which corresponds to the one used in this study (Figure 4), promotes the best results for determining the flexural strength of 3D printed elements. In this regard, Demiral et al. [26] highlight that the flexural strength of 3D-printed specimens tested in the perpendicular direction may be even higher than that reported for conventional (mould-casted) specimens.

In relation to the above and to compare the quality of the 3D printed specimens versus conventional mould-casted specimens, an ultrasonic pulse test was performed 28 days after curing according to the procedure described in the methodology (Section 2.3).

The results are presented in Table 5, where it is highlighted that the 3D printed specimens achieve an ultrasonic pulse velocity (CoW = 98.9%; CeW = 98.7%; RCBW = 98.2%) very similar to that of conventional specimens. Indeed, the ultrasonic pulse velocity of the 3D printed specimens corresponding to the CoW 0.30, CeW 0.33 and RCBW 0.38 mixes was 3114, 3313 and 3238 m/s, respectively. In comparison, the conventional specimens reported values of 3149 m/s (CoW), 3356 m/s (CeW) and 3297 m/s (RCBW).

Table 5. Results of the ultrasonic pulse test of the 3D printed and conventional (mold-casted) specimens.

| Mix | Cylinder | Ultrasonic Pulse Velocity (m/s) |
|-----------|--------------|---------------------------------|
| CoW 0.30 | 3D printed | 3114 ± 12 |
| | Mould-casted | 3149 ± 11 |
| CeW 0.33 | 3D printed | 3313 ± 10 |
| | Mould-casted | 3356 ± 23 |
| RCBW 0.38 | 3D printed | 3238 ± 12 |
| | Mould-casted | 3297 ± 13 |

According to the literature, the ultrasonic pulse velocity of concrete samples ranges from 3000 m/s (low quality concrete) to 5000 m/s (high quality concrete). In this regard, the speed of the ultrasonic pulse is directly related to the density of the material and to the mechanical properties. The quality shown by the 3D printed elements thus coincides with the physical-mechanical.

3.4.3. Microstructural Analysis

Additionally, the macroscopic (stereomicroscope) and microstructural (SEM) observation of the 3D printed specimens is presented in Figures 14–16 for the case of the CoW 0.30, CeW 0.33 and RCBW 0.38 mixes, respectively.

It is worth mentioning again that the specimens were printed with a fill percentage of 100%, obtaining a solid structure in which it is almost imperceptible to distinguish between one layer and another by visual inspection of the cross section of the specimens. Only at the edges of the specimen is it possible to distinguish the area of interface between layers and the superficial silhouette of each layer. The quality of the filling of the 3D specimens and their level of densification agrees with the results obtained using the ultrasonic pulse test (Table 5) and their similarity with the results reported by the conventional specimens (mould-casted).

A magnification ($50\times$) of the area of interface between layers allowed to corroborate the perfect adhesion between the layers and the obtaining of a solid and homogeneous structure in the CoW and CeW mixes, consistent with the physicomechanical performance of these specimens. In the case of the RCBW 0.38 mix, some cracks were identified in the area of interface between layers (directed) and inside the layers (non-directed), which may be associated with shrinkage and drying shrinkage phenomena promoted by the high L/S ratio (0.38) that this mix required for its 3D printing, and which in turn could have affected the mechanical performance of the 3D specimens (interlayer adhesion). According to Nodehi et al. [40], shrinkage is one of the main causes of the concentration of tensile and shear stresses in the area of interface between layers, and therefore of the generation of fissures and cracks in this area.

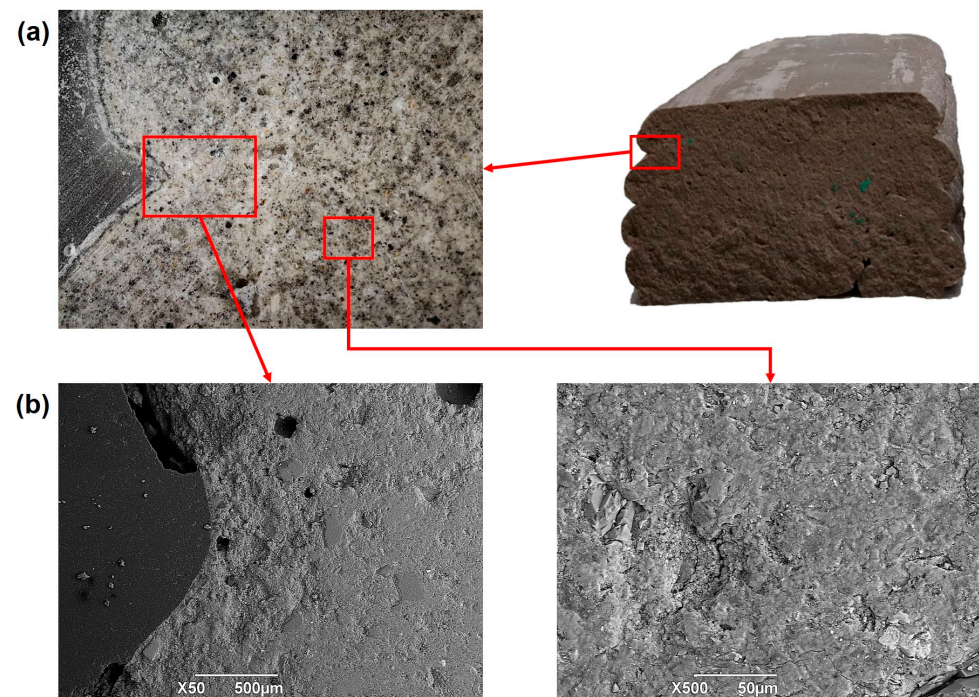


Figure 14. (a) Macroscopic (stereomicroscope), and (b) microstructural (SEM) observation of the interface zone between layers. Cross section of the CoW 0.30 3D printed specimen.

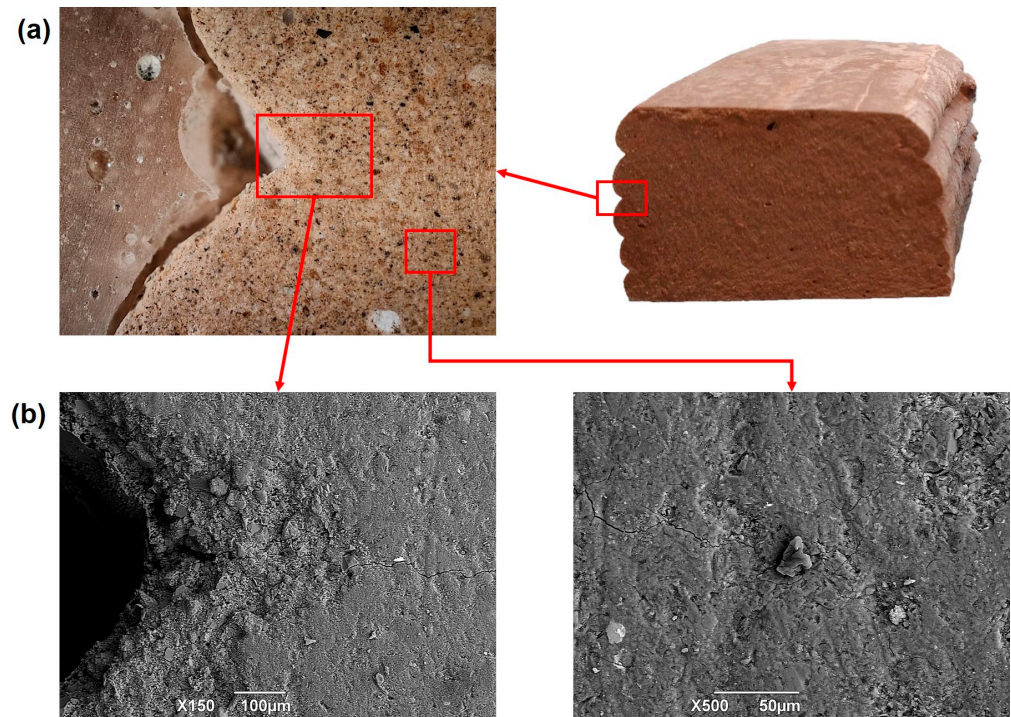


Figure 15. (a) Macroscopic (stereomicroscope), and (b) microstructural (SEM) observation of the interface zone between layers. Cross section of the CeW 0.33 3D printed specimen.

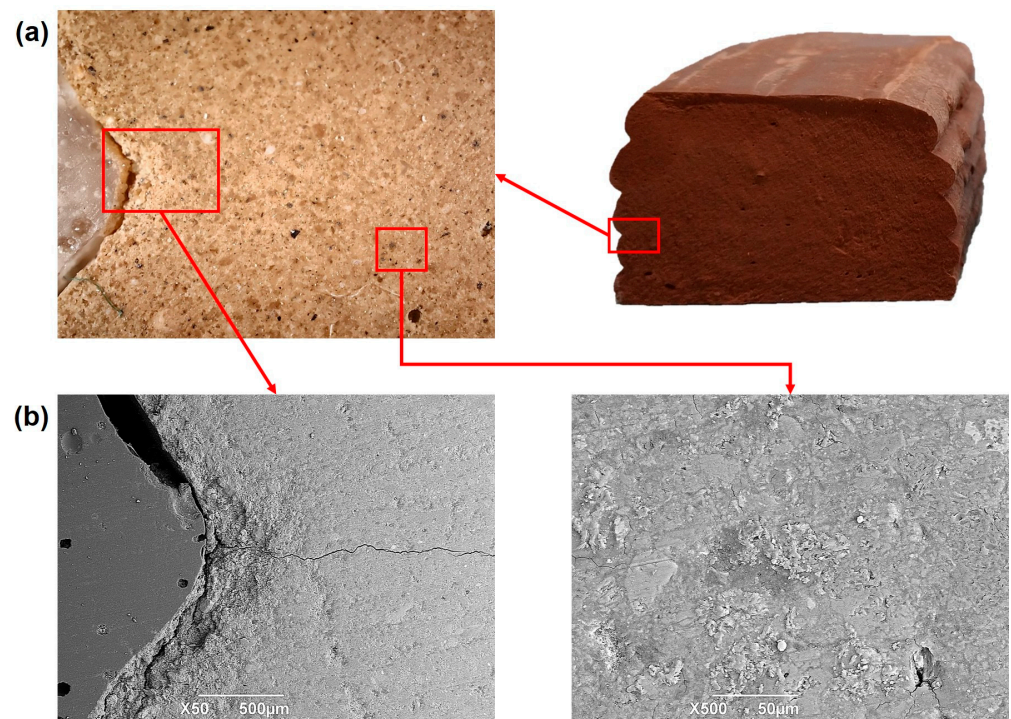


Figure 16. (a) Macroscopic (stereomicroscope), and (b) microstructural (SEM) observation of the interface zone between layers. Cross section of the RCBW 0.38 3D printed specimen.

4. Conclusions

The addition of 30% OPC and 4% Na₂SO₄ as chemical activator allowed the synthesis of hybrid cements based on 70% concrete waste (CoW), ceramic waste (CeW) and red clay brick waste (RCBW) with compressive strengths (25 °C, 90 days) up to 30.7, 37.0 and 33.2 MPa, respectively. Additionally, it was possible to demonstrate that the variation of the L/S ratio (0.30–0.38) affects the mechanical strength of hybrid cements, it being necessary to find a balance in relation to the properties in the fresh state necessary for its application in a 3D printing process.

The L/S ratio controls the properties in the fresh state (minislump, flowability index and buildability) of the mixes for 3D printing. A high L/S ratio promoted greater flowability and at the same time affected the buildability of the mixes. Very dry mixes meanwhile do not favour extrusion and 3D printing processes.

The type of waste influenced the rheological behavior of the mixes, being most fluid in the case of CoW, followed by CeW and finally RCBW. The RCBW demanded the greatest L/S ratio (0.38) among the waste studied to achieve the necessary flowability in 3D printing. The optimal L/S ratios for the CoW and CeW meanwhile were 0.30 and 0.33, respectively.

The results showed that the CoW, CeW and RCBW mixes that were found to have a minislump between 10–20 mm, flowability index between 2.0–2.4 and buildability greater than 80% were suitable for use in 3D printing processes.

The evaluation of the loss of workability (minislump and flowability) as a function of mixing time allowed us to determine that the open time of the CoW 0.30, CeW 0.33 and RCBW 0.38 mixes was 30, 20 and 10 min, respectively. These results were below the initial setting time reported for these same mixes (180–250 min). Moreover, the analysis of the ultrasonic pulse velocity during the fresh state made it possible to show that the mixes present microstructural changes before the initial setting time, which is consistent with the loss of workability (minislump and flowability) reported during the first minutes of reaction (≤ 30 min).

The CoW 0.30, CeW 0.33 and RCBW 0.38 mixes presented an adequate extrusion and 3D printing capacity, allowing to obtain portions with a good surface finish, without the presence of defects, discontinuities and/or pores. Meanwhile, the 3D printed cylinders (17 layers) made it possible to establish the high level of buildability of the mixes (close to 97–99%), managing to corroborate the results obtained by the mixes in the fresh state tests.

The 3D printed specimens (100% infill) achieved adequate physical-mechanical performance, with compressive strengths of 18.2 MPa (CoW 0.30), 27.7 MPa (CeW 0.33) and 21.7 MPa (RCBW 0.38) after 28 days of curing (25 °C), values that exceed the structural limit (≥ 17.5 MPa) established by the Colombian Regulations for Earthquake Resistant Construction (NSR-10) for concrete mixes.

The print quality of the mixes was confirmed using an ultrasonic pulse test (28 days). The CoW 0.30, CeW 0.33 and RCBW 0.38 mixes reported speed values of 3114, 3313 and 3238 m/s, respectively, results very similar to those obtained using conventional specimens (mold-casted). Microscopic observation (SEM) meanwhile revealed a dense interface and good quality interlayer adhesion for the case of the CoW 0.30 and CeW 0.33 mixes. In contrast, for the RCBW 0.38 mix, the presence of fissures and cracks in the interface between layers was identified to be a result of contraction and shrinkage phenomena due to drying, possibly promoted by the high L/S ratio of this mix (0.38). This finding suggests the possibility of studying (in future research) the control of this phenomenon through the incorporation of microfibers and particles.

Author Contributions: Conceptualization and methodology, R.R.-S. and R.M.d.G.; methodology and investigation, R.R.-S., F.M. and A.V.; writing—original draft preparation, R.R.-S.; supervision, project administration, funding acquisition, R.M.d.G.; writing—review and editing, R.R.-S. and R.M.d.G. All authors have read and agreed to the published version of the manuscript.

Funding: This research was funded by Ministry of Science Technology and Innovation (Minciencias) through Funding Call 6 of the 2021–2022 biennium of the General Royalties System (SGR) (BPIN 2020000100625).

Institutional Review Board Statement: Not applicable.

Informed Consent Statement: Not applicable.

Data Availability Statement: Not applicable.

Acknowledgments: The authors, members of the Composite Materials Group (CENM), thank the project “Development of a 3D printing system of sustainable non-conventional materials for the advancement of rural infrastructure in the department of Cauca” of the Universidad del Valle, financed by the Ministry of Science Technology and Innovation (Minciencias).

Conflicts of Interest: The authors declare no conflict of interest.

References

1. Grand View Research 3D Printing Construction Market Size, Share & Trends Analysis Report by Construction Method (Extrusion, Powder Bonding), by Material Type (Concrete, Metal), by End-User (Building, Infrastructure), and Segment Forecasts, 2022–2030. Available online: <https://www.grandviewresearch.com/industry-analysis/3d-printing-constructions-market> (accessed on 24 November 2022).
2. Ma, G.; Wang, L.; Ju, Y. State-of-the-Art of 3D Printing Technology of Cementitious Material—An Emerging Technique for Construction. *Sci. China Technol. Sci.* **2018**, *61*, 475–495. [\[CrossRef\]](#)
3. De Schutter, G.; Lesage, K.; Mechtcherine, V.; Nerella, V.N.; Habert, G.; Agusti-Juan, I. Vision of 3D Printing with Concrete—Technical, Economic and Environmental Potentials. *Cem. Concr. Res.* **2018**, *112*, 25–36. [\[CrossRef\]](#)
4. Alhumayani, H.; Gomaa, M.; Soebarto, V.; Jabi, W. Environmental Assessment of Large-Scale 3D Printing in Construction: A Comparative Study between Cob and Concrete. *J. Clean. Prod.* **2020**, *270*, 122463. [\[CrossRef\]](#)
5. Weng, Y.; Li, M.; Ruan, S.; Wong, T.N.; Tan, M.J.; Ow Yeong, K.L.; Qian, S. Comparative Economic, Environmental and Productivity Assessment of a Concrete Bathroom Unit Fabricated through 3D Printing and a Precast Approach. *J. Clean. Prod.* **2020**, *261*, 121245. [\[CrossRef\]](#)
6. Sanjayan, J.G.; Nematollahi, B. Chapter 1—3D Concrete Printing for Construction Applications. In *3D Concrete Printing Technology*; Sanjayan, J.G., Nazari, A., Nematollahi, B., Eds.; Butterworth-Heinemann: Oxford, UK, 2019; pp. 1–11, ISBN 978-0-12-815481-6.
7. Robayo-Salazar, R.; Mejía de Gutiérrez, R.; Villaquirán-Cacedo, M.A.; Delvasto Arjona, S. 3D Printing with Cementitious Materials: Challenges and Opportunities for the Construction Sector. *Autom. Constr.* **2023**, *146*, 104693. [\[CrossRef\]](#)
8. Bhattacharjee, S.; Basavaraj, A.S.; Rahul, A.V.; Santhanam, M.; Gettu, R.; Panda, B.; Schlangen, E.; Chen, Y.; Copuroglu, O.; Ma, G.; et al. Sustainable Materials for 3D Concrete Printing. *Cem. Concr. Compos.* **2021**, *122*, 104156. [\[CrossRef\]](#)
9. Gökçe, H.S.; Tuyan, M.; Nehdi, M.L. Alkali-Activated and Geopolymer Materials Developed Using Innovative Manufacturing Techniques: A Critical Review. *Constr. Build. Mater.* **2021**, *303*, 124483. [\[CrossRef\]](#)
10. Zhong, H.; Zhang, M. 3D Printing Geopolymers: A Review. *Cem. Concr. Compos.* **2022**, *128*, 104455. [\[CrossRef\]](#)
11. Raza, M.H.; Zhong, R.Y.; Khan, M. Recent Advances and Productivity Analysis of 3D Printed Geopolymers. *Addit. Manuf.* **2022**, *52*, 102685. [\[CrossRef\]](#)
12. Lazorenko, G.; Kasprzhitskii, A. Geopolymer Additive Manufacturing: A Review. *Addit. Manuf.* **2022**, *55*, 102782. [\[CrossRef\]](#)
13. Khan, M.A. Mix Suitable for Concrete 3D Printing: A Review. *Mater. Today Proc.* **2020**, *32*, 831–837. [\[CrossRef\]](#)
14. Xia, M.; Sanjayan, J. Method of Formulating Geopolymer for 3D Printing for Construction Applications. *Mater. Des.* **2016**, *110*, 382–390. [\[CrossRef\]](#)
15. Robayo-Salazar, R.A.; Mejía de Gutiérrez, R. Natural Volcanic Pozzolans as an Available Raw Material for Alkali-Activated Materials in the Foreseeable Future: A Review. *Constr. Build. Mater.* **2018**, *189*, 109–118. [\[CrossRef\]](#)
16. Zhao, J.; Tong, L.; Li, B.; Chen, T.; Wang, C.; Yang, G.; Zheng, Y. Eco-Friendly Geopolymer Materials: A Review of Performance Improvement, Potential Application and Sustainability Assessment. *J. Clean. Prod.* **2021**, *307*, 127085. [\[CrossRef\]](#)
17. Shehata, N.; Mohamed, O.A.; Sayed, E.T.; Abdelkareem, M.A.; Olabi, A.G. Geopolymer Concrete as Green Building Materials: Recent Applications, Sustainable Development and Circular Economy Potentials. *Sci. Total Environ.* **2022**, *836*, 155577. [\[CrossRef\]](#)
18. Ouellet-Plamondon, C.; Habert, G. Life Cycle Assessment (LCA) of Alkali-Activated Cements and Concretes. In *Handbook of Alkali-Activated Cements, Mortars and Concretes*; Woodhead Publishing: Sawston, UK, 2015; pp. 663–686, ISBN 9781782422761.
19. Valencia-Saavedra, W.; Robayo-Salazar, R.; Mejía de Gutiérrez, R. Alkali-Activated Hybrid Cements Based on Fly Ash and Construction and Demolition Wastes Using Sodium Sulfate and Sodium Carbonate. *Molecules* **2021**, *26*, 7572. [\[CrossRef\]](#)
20. Joseph, S.; Snellings, R.; Cizer, Ö. Activation of Portland Cement Blended with High Volume of Fly Ash Using Na₂SO₄. *Cem. Concr. Compos.* **2019**, *104*, 103417. [\[CrossRef\]](#)
21. Donatello, S.; Fernández-Jimenez, A.; Palomo, A. Very High Volume Fly Ash Cements. Early Age Hydration Study Using Na₂SO₄ as an Activator. *J. Am. Ceram. Soc.* **2013**, *96*, 900–906. [\[CrossRef\]](#)

22. Robayo-Salazar, R.; Valencia-Saavedra, W.; Gutiérrez, R.M. Reuse of Powders and Recycled Aggregates from Mixed Construction and Demolition Waste in Alkali-Activated Materials and Precast Concrete Units. *Sustainability* **2022**, *14*, 9685. [[CrossRef](#)]
23. Robayo-Salazar, R.; Valencia-Saavedra, W.; Mejía de Gutiérrez, R. Recycling of Concrete, Ceramic, and Masonry Waste via Alkaline Activation: Obtaining and Characterization of Hybrid Cements. *J. Build. Eng.* **2022**, *46*, 103698. [[CrossRef](#)]
24. Şahin, O.; İlcan, H.; Ateşli, A.T.; Kul, A.; Yıldırım, G.; Şahmaran, M. Construction and Demolition Waste-Based Geopolymers Suited for Use in 3-Dimensional Additive Manufacturing. *Cem. Concr. Compos.* **2021**, *121*, 104088. [[CrossRef](#)]
25. İlcan, H.; Sahin, O.; Kul, A.; Yildirim, G.; Sahmaran, M. Rheological Properties and Compressive Strength of Construction and Demolition Waste-Based Geopolymer Mortars for 3D-Printing. *Constr. Build. Mater.* **2022**, *328*, 127114. [[CrossRef](#)]
26. Demiral, N.C.; Ozkan Ekinci, M.; Sahin, O.; Ilcan, H.; Kul, A.; Yildirim, G.; Sahmaran, M. Mechanical Anisotropy Evaluation and Bonding Properties of 3D-Printable Construction and Demolition Waste-Based Geopolymer Mortars. *Cem. Concr. Compos.* **2022**, *134*, 104814. [[CrossRef](#)]
27. ASTM C230/230M-20; Standard Specification for Flow Table for Use in Tests of Hydraulic Cement. American Society for Testing and Materials (ASTM): West Conshohocken, PA, USA, 2020.
28. ASTM C191-21; Standard Test Methods for Setting of Hydraulic Cement by Vicat Needle. American Society for Testing and Materials (ASTM): West Conshohocken, PA, USA, 2021.
29. UNE EN 1015:2020; Methods of Test for Mortar for Masonry-Part 11: Determination of Flexural and Compressive Strength of Hardened Mortar. AENOR: Madrid, Spain, 2020.
30. ASTM C642-13; Standard Test Method for Density, Absorption, and Voids in Hardened Concrete. American Society for Testing and Materials (ASTM): West Conshohocken, PA, USA, 2013.
31. ASTM C597-16; Standard Test Method for Pulse Velocity Through Concrete. American Society for Testing and Materials (ASTM): West Conshohocken, PA, USA, 2016.
32. Souza, M.T.; Ferreira, I.M.; de Moraes, E.G.; Senff, L.; Arcaro, S.; Pessôa, J.R.C.; Ribeiro, M.J.; de Oliveira, A.P.N. Role of Chemical Admixtures on 3D Printed Portland Cement: Assessing Rheology and Buildability. *Constr. Build. Mater.* **2022**, *314*, 125666. [[CrossRef](#)]
33. Tay, Y.W.D.; Qian, Y.; Tan, M.J. Printability Region for 3D Concrete Printing Using Slump and Slump Flow Test. *Compos. Part B* **2019**, *174*, 106968. [[CrossRef](#)]
34. Kaliyavaradhan, S.K.; Ambily, P.S.; Prem, P.R.; Ghodke, S.B. Test Methods for 3D Printable Concrete. *Autom. Constr.* **2022**, *142*, 104529. [[CrossRef](#)]
35. Uppalapati, S.; Vandewalle, L.; Cizer, Ö. Monitoring the Setting Process of Alkali-Activated Slag-Fly Ash Cements with Ultrasonic P-Wave Velocity. *Constr. Build. Mater.* **2021**, *271*, 121592. [[CrossRef](#)]
36. Ranjbar, N.; Mehrali, M.; Kuenzel, C.; Gundlach, C.; Pedersen, D.B.; Dolatshahi-Pirouz, A.; Spangenberg, J. Rheological Characterization of 3D Printable Geopolymers. *Cem. Concr. Res.* **2021**, *147*, 106498. [[CrossRef](#)]
37. Zhang, Y.; Zhang, Y.; She, W.; Yang, L.; Liu, G.; Yang, Y. Rheological and Harden Properties of the High-Thixotropy 3D Printing Concrete. *Constr. Build. Mater.* **2019**, *201*, 278–285. [[CrossRef](#)]
38. Sika 3D CONCRETE PRINTING: Sikacrete® 3D Materials for Fast and Precisely Printed Concrete. Available online: <https://www.sika.com/en/knowledge-hub/3d-concrete-printing.html#sika> (accessed on 24 November 2022).
39. Che, Y.; Yang, H. Hydration Products, Pore Structure, and Compressive Strength of Extrusion-Based 3D Printed Cement Pastes Containing Nano Calcium Carbonate. *Case Stud. Constr. Mater.* **2022**, *17*, e01590. [[CrossRef](#)]
40. Nodehi, M.; Aguayo, F.; Nodehi, S.E.; Gholampour, A.; Ozbakkaloglu, T.; Gencel, O. Durability Properties of 3D Printed Concrete (3DPC). *Autom. Constr.* **2022**, *142*, 104479. [[CrossRef](#)]

Disclaimer/Publisher’s Note: The statements, opinions and data contained in all publications are solely those of the individual author(s) and contributor(s) and not of MDPI and/or the editor(s). MDPI and/or the editor(s) disclaim responsibility for any injury to people or property resulting from any ideas, methods, instructions or products referred to in the content.